

Measurement of Heat Flux with Calorimeters in the D-Module of GAMMA 10/PDX^{*)}

Miki IWAMOTO, Yousuke NAKASHIMA, Hiroto MATSUURA¹⁾, Hisato TAKEDA, Katsuhiro HOSOI, Kazuya ICHIMURA, Satoru KIGURE, Shigehito TAKAHASHI, Yasunari HOSODA, Kensuke OKI, Yu NAGATSUKA, Motoki YOSHIKAWA, Ryo NOHARA, Mizuki SAKAMOTO, Tsuyoshi IMAI and Makoto ICHIMURA

Plasma Research Center, University of Tsukuba, Tsukuba, Ibaraki 305-8577, Japan

¹⁾*Radiation Research Center, Osaka Prefecture University, Osaka 599-8570, Japan*

(Received 11 December 2013 / Accepted 28 April 2014)

In the GAMMA 10/PDX tandem mirror device at the University of Tsukuba, divertor simulation experiments were conducted for realizing detached plasma. A divertor simulation experimental module (D-module), in which a V-shaped target is mounted, was installed in the west end-cell of GAMMA 10/PDX. The spatial distribution of the heat flux was measured with calorimeters on the V-shaped target under target angle conditions of 30°, 45° and 60°. The spatial distribution depends on the structure of magnetic field in the end-cell. The heat flux depended on the gas species and the amount of gas injection was also investigated. With increasing Ar gas pressure, the ion flux decreased by approximately a factor of four, whereas the heat flux decreased by three fifths.

© 2014 The Japan Society of Plasma Science and Nuclear Fusion Research

Keywords: GAMMA 10/PDX, D-module, calorimeter, heat flux, detached plasma, divertor, neutral gas injection, V-shaped target, ion flux, plasma and neutral interaction

DOI: 10.1585/pfr.9.3402121

1. Introduction

In toroidal fusion devices, the divertor is exposed to high heat load of tens of MW at steady state conditions. To reduce the heat flux on the divertor plate, it is necessary to enhance radiation cooling by neutral gas and produce detached plasma in the divertor region [1–3]. Divertor simulation experiments were conducted using the high heat flux out of the end-mirror in the GAMMA 10/PDX tandem mirror device at the University of Tsukuba [4–7]. To investigate interactions between end-loss plasma and divertor materials, a V-shaped divertor target plate is mounted in the newly designed divertor simulation experimental module (D-module) installed at the exit of the west end-mirror of GAMMA 10/PDX. The main purpose of this study is to realize the detached plasma in the D-module. The advantage of performing divertor simulation experiments in GAMMA 10/PDX is that high-energy plasma with ion temperatures of 100–400 eV can be generated using various plasma-heating devices [8,9]. The highest heat flux ($> 10 \text{ MW/m}^2$) was obtained under strong magnetic field ($\sim 1 \text{ T}$) using high-power electron cyclotron heating (ECH). Therefore, we performed experiments under the plasma parameter region that is similar to the SOL plasma of toroidal fusion device, such as ITER. In this study, the spatial distribution of the heat flux was investigated with and without neutral gas (H_2 , Ar) injection on the V-shaped

target plate in the D-module. In sections 2 and 3, the experimental set up of the GAMMA 10/PDX, D-module and calorimeter is described. Experimental results are discussed in section 4 and the summary is presented in section 5.

2. GAMMA 10/PDX and D-Module

Figure 1 (a) shows the GAMMA 10/PDX, which consists of a central-cell with a simple mirror configuration, minimum-B anchor-cells and a plug/barrier-cell for potential confinement. Plasma is mainly generated in the central-cell. Plasma-heating systems are composed of ion cyclotron range of frequencies (ICRF), neutral beam injection and ECH. In the central-cell, high-temperature plasma ($T_i \sim 4 \text{ keV}$, $n_e \sim 10^{18} \text{ m}^{-3}$) can be generated by applying ICRF. On the other hand, ECH can generate high-temperature electrons (100 eV). The end-loss plasma, which escapes from the central-cell, passes through the anchor-cell, plug/barrier-cell and reaches the end-cell.

The D-module has been installed in the west end-cell of GAMMA 10/PDX. Because the D-module can be moved up on the machine center axis and down to the bottom of the vacuum chamber using the elevating system shown in Fig. 1 (b), both divertor simulation and conventional mirror plasma experiments can be conducted. In a typical experiment, we use magnetoplasma dynamic (MPD) arc jet-type plasma injectors for the first plasma start-up, which are located in both ends of GAMMA 10/PDX [10]. In the D-module experiments, we only use

author's e-mail: iwamoto_miki@prc.tsukuba.ac.jp

^{*)} This article is based on the presentation at the 23rd International Toki Conference (ITC23).

the east-side MPD arc jet. ICRF heating is performed in the central-cell and high-temperature plasma is generated.

The graph and detailed components of the D-module are shown in Fig. 2. The D-module consists of a V-shaped target system made of tungsten and is enclosed by a rectangular box made of stainless steel. In front of the box, a plasma inlet aperture is installed. The angle of the target plate (α_v) varies from 15° to 80° . Argon gas injection ports, 13 calorimeters to measure the heat flux from the end-loss plasma flow and Langmuir probes are installed on the target plate. A calorimeter and probe pair is also installed at the corner of the V-shaped target. Two spectrometers are attached outside the end-cell vacuum vessel to view the line emission in front of the V-shaped target. A H_2 gas injection port is also installed in the plasma upstream side of the D-module, as shown in Fig. 2 (c).

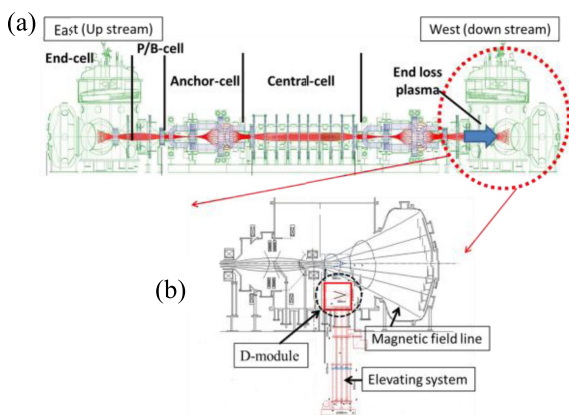


Fig. 1 Schematic view of (a) the GAMMA 10/PDX vacuum vessels and (b) west-end vacuum vessel and D-module system.

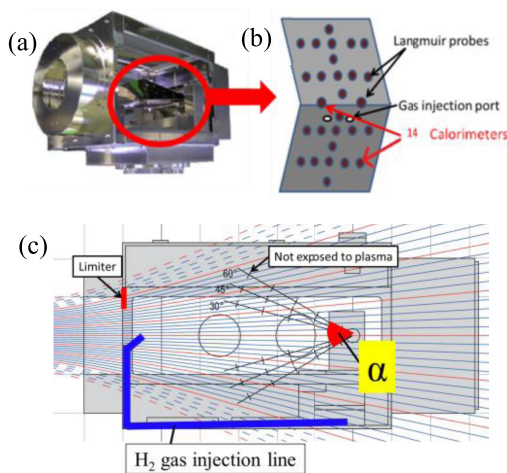


Fig. 2 Image (a) of the D-module, (b) V-shaped target and calorimeters on the lower surface of the target, (c) side view of the D-module and the shape of the magnetic field line and location of the H_2 gas injection port.

3. Heat Flux Evaluation

The heat flux is measured with the calorimeter attached on the V-shaped target is evaluated from the temperature increments (ΔT [K]) of the stainless steel substrate (φ 10 mm, 0.2 mm in thickness) before and after the plasma discharge. We measure ΔT using a thermocouple and the heat quantity Q J received by the substrate is

$$Q = mC\Delta T, \tag{1}$$

where m is the mass of the stainless steel and C [J/kg K] is the heat capacity. The measured heat flux is

$$P = \frac{Q}{tS} \times 10^{-6} \text{ [MW/m}^2\text{]}, \tag{2}$$

where t is the plasma exposure time, S is the effective collection area of the heat and S' is the substrate surface area. The relation between S and S' is

$$S = S' \sin \gamma, \tag{3}$$

where γ is the incident angle of the magnetic field lines to the substrate.

4. Experimental Results and Discussion

4.1 Distribution of heat flux

Thirteen calorimeters are installed in the Y and Z directions on the target plate. As shown in Fig. 3, the alignment of the detectors consists of two arrays in the Y direction (Line (a) and Line (b)) and one array in the Z direction (Line (c)). The spatial distribution of the heat flux on the target plate was measured with the calorimeter under target angle (α_v) conditions of 30° , 45° and 60° .

Figures 4 and 5 show the spatial profiles of the heat flux in the Y -direction at different Z positions (Lines (a) and (b)). Data points connected with lines show the model results determined by considering the magnetic structure in the end-cell and incident angle γ . In the model, it is assumed that the total heat flux depends on the ion energy and particle density, which is inversely proportional to the area of the flux tube along the Z direction and has Gaussian distribution in the radial direction. It was found that each heat flux profile in lines (a) and (b) peaks at $Y = 0$ and decreases toward the Y direction. The calculation results

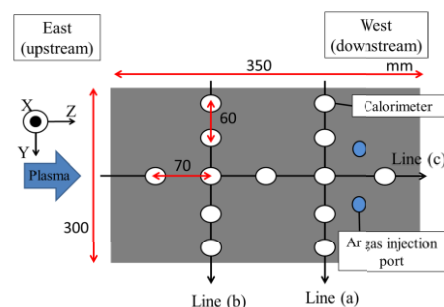


Fig. 3 Schematic view of the calorimeters array.

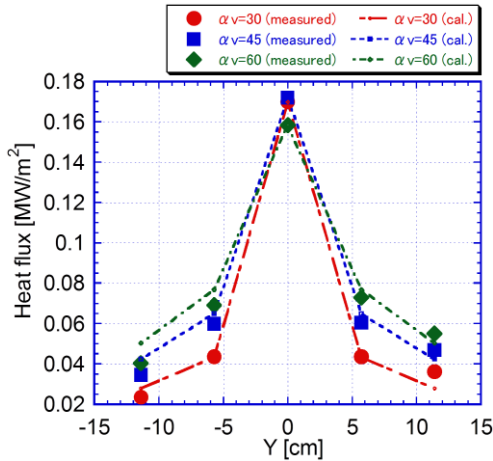


Fig. 4 Heat flux distribution on line (a).

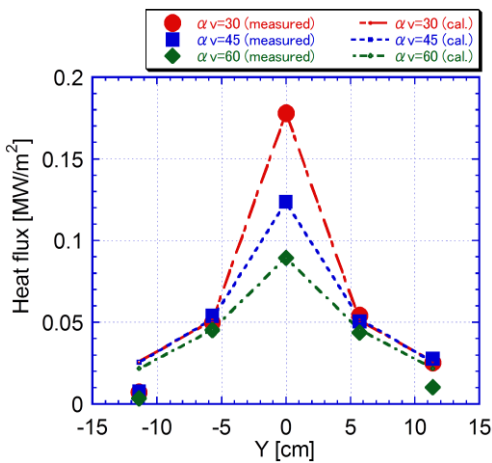


Fig. 5 Heat flux distribution on line (b).

are normalized at $Y = 0$. The close relation between these results and the magnetic field line is confirmed; that is, the end-loss plasma flows out according to the magnetic field line structure because the magnetic flux tube in the end-cell spreads radially toward the Z direction.

The heat flux has a steep profile around $Y = 0$ [cm]. This is owing to the shape of the magnetic flux tube and incidence angle γ of the magnetic field line to the target. The angle γ has a minimum at $Y = 0$. For example, for $\alpha_v = 30^\circ$, γ is 25° and 80° at $Y = 0$ cm and $Y = 5.7$ cm, respectively. The trends resemble the calculated values.

Figure 6 shows the spatial profile of the heat flux in the Z direction and position coordinates of calorimeters for α_v . For a small angle α_v (30°), the observed heat flux is almost flat, whereas for a large angle of α_v (60°), strong reduction in the heat flux is observed near the plasma limiter located at the inlet aperture. This can be attributed to the magnetic flux tube that is scraped off by the plasma inlet aperture in the case of a large angle. This trend does not appear in the calculations as the inlet is not considered.

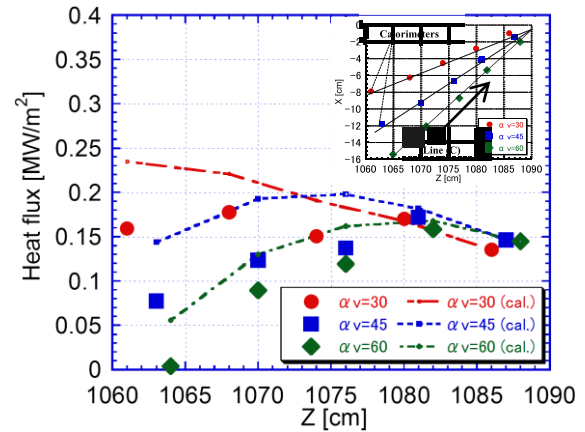

 Fig. 6 Spatial profile of the heat flux in the Z direction and position coordinates of calorimeters corresponding to α_v .

Table 1 Data for gas injection parameters.

	H ₂	Ar
Delay [s]	-0.3	-0.3
Pulse width [s]	0.2	0.2
Plenum pressure [10^4 Pa]	9.9	5/10

4.2 Neutral gas injection

To increase the plasma density and enhance radiation cooling in the D-module, hydrogen and argon gases are injected during plasma exposure. Owing to the low conductance of the gas introducing tube, the gases are injected sub seconds before plasma ignition. The timing data for the gas injection are listed in Table 1.

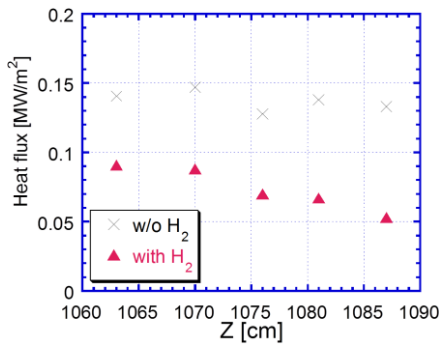
4.2.1 H₂ gas injection

Figure 7 shows the heat flux distribution in the H₂ gas injection experiment. In this figure, the heat flux data measured on line (c) are plotted for the cases with and without H₂ gas injection for $\alpha_v = 45^\circ$. In this experiment, the ICRF power is larger than that of the experiment shown in Fig. 6, and the ECH is applied on the latter half of the discharge. Consequently, the measured diamagnetism is approximately three times higher than that in Fig. 6.

The heat flux decreases at all Z positions in the case of H₂ gas injection. The difference in heat flux between the case of H₂ gas injection and without gas injection is enhanced in the downstream region of the plasma. The above dependence is explained in the following manner. From the electron density measurements using the Langmuir probes during H₂ gas injection, the electron density and temperature in the upstream region are higher than those in the downstream region, as shown in Table 2. Simultaneously, plasma-neutral gas interaction is taking place around the plasma upstream region, owing to the H₂ gas injection in the D-module. An area of ionization is created near the plasma inlet aperture as the H₂ gas uniformly fills the module. Therefore, the heat flux in the penetrating ionization

Table 2 Electron density and temperature with and without H₂ gas.

	Upstream	Downstream
n_e [m ⁻³] (w/o H ₂)	1.7×10^{16}	3.6×10^{16}
n_e [m ⁻³] (with H ₂)	7.03×10^{16}	3.85×10^{16}
T_e [eV] (w/o H ₂)	27.5	18.9
T_e [eV] (with H ₂)	5.4	4.2


 Fig. 7 Heat flux distribution in the cases with and without H₂ gas.

area is significantly reduced.

4.2.2 Ar gas injection

Figure 8 shows the heat flux versus plenum pressure dependence of Ar gas on line (c). In this experiment, H₂ and Ar gases are simultaneously injected for $\alpha_v = 45^\circ$.

The heat flux decreases at every position as the Ar gas pressure increases. The ion flux is also measured using a Langmuir probe at the corner of the V-shaped target. The ion flux decreases about a factor of four and the heat flux decreases by three fifths owing to the Ar gas injection. From the electron density measurement with the Langmuir probes, which is nearest to the corner of the V-shaped target, the electron density is $1.6 \times 10^{17} \text{ m}^{-3}$ without Ar gas and slightly reduced to $1.4 \times 10^{17} \text{ m}^{-3}$ with Ar gas. From the reduction in the ion flux and electron density, it is estimated that the flow velocity is reduced to 30% owing to Ar gas injection. In the case of only H₂ gas injection, charge exchange is thought to dominate the dissipation mechanisms of ion energy. However, in the case of simultaneous injection of H₂ and Ar gases, it is suggested that radiation cooling is enhanced and the cooling of electrons is facilitated by Ar injection. A more quantitative evaluation will be presented in the future.

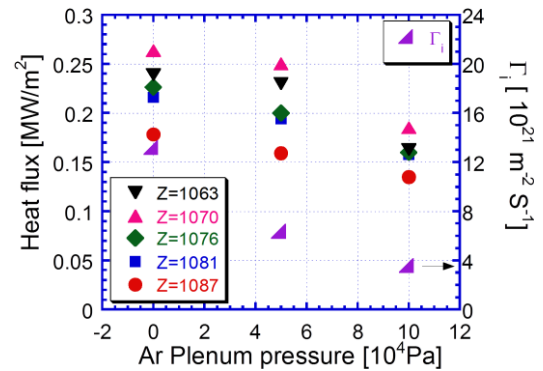


Fig. 8 Heat flux vs. plenum pressure for line (c) in the Ar gas injection experiment.

5. Summary

The spatial distribution of the heat flux along the target plate was measured with calorimeters for target angle α_v of 30° , 45° and 60° . The heat flux decreased at all points in the case that H₂ gas was injected at $\alpha_v = 45^\circ$. Under simultaneous injection of H₂ and Ar gases, the heat and ion fluxes decreased with increasing Ar gas pressure. From the results, favorable conditions for detached plasma were obtained.

Acknowledgement

This study was supported by the bi-directional collaboration research program of the University of Tsukuba, National Institute for Fusion Science, Osaka Prefecture University (NIFS12KUGM066, NIFS11KUGM050 and NIFS12KUGM071). The authors thank the members of the GAMMA 10 groups for their collaboration in the experiments and for their helpful discussions.

- [1] K. Shimizu *et al.*, J. Plasma Fusion Res. **80**, 183 (2004) (in Japanese).
- [2] S. Masuzaki *et al.*, J. Plasma Fusion Res. **80**, 201 (2004) (in Japanese).
- [3] M. Shimada, J. Plasma Fusion Res. **80**, 222 (2004) (in Japanese).
- [4] Y. Nakashima *et al.*, Fusion Eng. Des. **85**, Issue 6, 956 (2010).
- [5] Y. Nakashima *et al.*, Trans. Fusion Sci. Technol. **59**, No.1T, 61 (2011).
- [6] T. Imai *et al.*, J. Plasma Fusion Res. **87**, 752 (2011) (in Japanese).
- [7] Y. Nakashima *et al.*, J. Nucl. Mater. **438**, S738 (2013).
- [8] H. Takeda *et al.*, Plasma Fusion Res. **7**, 2405151 (2012).
- [9] K. Ichimura *et al.* Plasma Fusion Res. **7**, 2405147 (2012).
- [10] K. Nemoto *et al.* Fusion Sci. Technol. **51**, 223 (2013).